



## Two-dimensional numerical modeling of pressure–temperature–time paths for the exhumation of some granulite facies terrains in the Precambrian

Taras V. Gerya<sup>a</sup>, Leonid L. Perchuk<sup>a,b</sup>, Dirk D. van Reenen<sup>c,\*</sup>, C. Andre Smit<sup>c</sup>

<sup>a</sup>*Institute of Experimental Mineralogy, Russian Academy of Sciences, Chernogolovka, Moscow 142432, Russia*

<sup>b</sup>*Department of Petrology, Geological Faculty, Moscow State University, Vorobievsky Gory, Moscow 119899, Russia*

<sup>c</sup>*Department of Geology, Rand Afrikaans University, Auckland Park, South Africa*

Received 30 September 1998; accepted 16 June 1999

### Abstract

Pressure ( $P$ )–temperature ( $T$ ) paths accurately record movement of metamorphic rocks within the Earth's crust. 1D geodynamic modeling of  $P$ – $T$ –time paths of regional metamorphism have explained many important features of the  $P$ – $T$  evolution of metamorphic rocks. Further progress may be achieved using 2D numerical geodynamic modeling. Different types of  $P$ – $T$  paths obtained for some granulites allow their 2D numerical modeling in terms of a theory of gravitational redistribution of material within the Earth's crust. This modeling was done using the finite differences method for a Newtonian incompressible fluid. The  $P$ – $T$  paths obtained geothermobarometrically for metapelites from the Limpopo granulite complex were compared with the  $P$ – $T$ –time paths calculated numerically by monitoring the movement of different 'samples' in the thermal and gravitational field. The results of this monitoring support a hypothesis of isobaric cooling of granulites during the thermal interaction between rising hot granulites and sinking cool cratonic rocks. Effective viscosities of the rocks were gradually adjusted during the modeling by using the shape of the  $P$ – $T$  paths. The calculated average viscosity of  $10^{19}$  Pa s for the granulites, supports an idea that the lower crust is a weak layer between upper crust ( $10^{21}$  Pa s) and the Upper Mantle. The average rate of exhumation of granulites during the gravitational redistribution process is estimated at about 2.5 mm per year. This suggests exhumation of granulites from depths of about 30 km during approximately 10 Myr. The results of numerical modeling successfully explain the presence of two types of  $P$ – $T$  paths observed in metapelites of the Limpopo

\* Corresponding author.

*E-mail addresses:* taras@iem.ac.ru (T.V. Gerya), llp@geol.msu.ru (L.L. Perchuk), ddvr@na.rau.ac.za (D.D. van Reenen).

granulite complex emplaced between the > 3 Ga Kaapvaal and Zimbabwe cratons at ~2.65 Ga. © 2000 Elsevier Science Ltd. All rights reserved.

*Keywords:*  $P$ – $T$  paths; Metamorphic evolution; Granulites; Numerical modeling; Precambrian crust; Exhumation mechanisms

---

## 1. Introduction

The pressure ( $P$ )–temperature ( $T$ ) path is a direct record of the movement of a rock within the Earth's crust during the process of regional metamorphism. This suggests that  $P$ – $T$  paths are powerful tools in understanding some geodynamic processes (e.g., Perchuk, 1973, 1977; England and Thompson, 1984; Thompson and England, 1984; Spear, 1993). In the last 25 years, many  $P$ – $T$  paths were obtained for metamorphic complexes of different facies of regional metamorphism (for references see Spear, 1993). 1D geodynamic modeling of  $P$ – $T$ -time paths of regional metamorphism (England and Thompson, 1984) explained many important features of the  $P$ – $T$  evolution of metamorphic rocks, but further progress will depend on 2D and 3D numerical geodynamic modeling. This is especially relevant in the case of rocks with different  $P$ – $T$  paths occurring within the same metamorphic complex. The results of modeling should be applied to such metamorphic complexes where rocks with different types of  $P$ – $T$  paths have already been documented through detailed petrological and geothermobarometric studies.

This paper concentrates on granulite facies terrains for the following reasons:

1. Only retrograde  $P$ – $T$  paths are properly documented in granulites. This empirical rule follows from very simple physical laws: an increase in temperature (particularly above 700°C) leads to an increase in the entropy of a system and in the diffusion rate. As a result, the majority of reaction textures formed during the prograde stage of metamorphism are erased and only the post  $T$ -peak metamorphic history is preserved. Thus, the numerical geodynamic study of  $P$ – $T$ -time paths might only address the process of exhumation and cooling of granulite facies terrains.
2. On the basis of a review of 90 granulite facies terrains Harley (1989) showed that two major types of retrograde  $P$ – $T$  paths are typical for the complexes: (i) near isobaric cooling  $P$ – $T$  paths, and (ii) near isothermal decompression  $P$ – $T$  paths. Numerical modeling can therefore be restricted to only two major types of  $P$ – $T$  paths.
3. The rocks composing granulite complexes represent the ductile lower crust. This crust is sandwiched as a weak layer between a brittle-frictional upper crust and a harder lithospheric upper mantle (Ranalli, 1995). The position of the granulite material provides a high degree of mobility during the thermal granulite facies event. This allows the application of gravitational instability forces (Ramberg, 1981) to a process of exhumation of granulites associated with greenstone belts. A gravitational redistribution model (Perchuk, 1989) for the exhumation of such granulites was generally supported by 2D numerical modeling (Perchuk et al., 1992), thus creating a basis for further numerical studies.

One of the interesting granulite complexes providing a basis for numerical modeling is the

Limpopo granulite belt of Southern Africa. The  $\sim 2.65$  Ga Limpopo granulite belt is mainly composed of tonalitic gneisses and metapelites with some mafic and ultramafic gneisses, and it is located between the  $> 3$  Ga Kaapvaal and Zimbabwe cratons (van Reenen and Smit, 1996; van Reenen et al., 1990). Some granulites of the Limpopo complex represent high-grade metamorphic equivalents of typical Archean greenstone lithologies (e.g., van Reenen et al., 1990; van Reenen and Smit, 1996). The Limpopo complex is bounded by regional ductile shear zones developed after cratonic rocks and dipping under the high grade terrain. Non-isobaric metamorphic zoning is developed in those shear zones located between the Limpopo terrain and both cratons (Roering et al., 1992; van Reenen and Smit, 1996). The crust beneath the Limpopo belt (30–35 km thick) is thinner than under the adjacent Kaapvaal and Zimbabwe cratons (40–45 km) (Roering et al., 1992). The cratons show a clear stratigraphic sequence (De Wit and Ashwal, 1997), the lower part of which is mainly composed of gray gneisses, while the uppermost portion contains greenstone belts with abundant mafic-ultramafic volcanics and plutonics metamorphosed under conditions of amphibolite to greenschists facies. This defines a potential gravitational instability of the cratonic succession. The heating of the lower portion of such a crust to granulite facies conditions could result in the process of gravitational redistribution.

Perchuk et al. (1996) showed that two groups of  $P$ – $T$  paths can be deduced from preserved reaction textures (local mineral equilibria) and mineral zonation in the Limpopo granulite complex: (i) decompression cooling  $P$ – $T$  paths (Fig. 1a), and (ii) near isobaric cooling  $P$ – $T$  paths (Fig. 1b). The first type reflects evolution of  $P$ – $T$  conditions for several samples collected far ( $\sim 50$  km) from the boundary with the Kaapvaal craton, while the second one represents samples collected close to the boundary with the craton.

Perchuk et al. (1996) explained the existence of the two groups of  $P$ – $T$  paths (Fig. 1) by

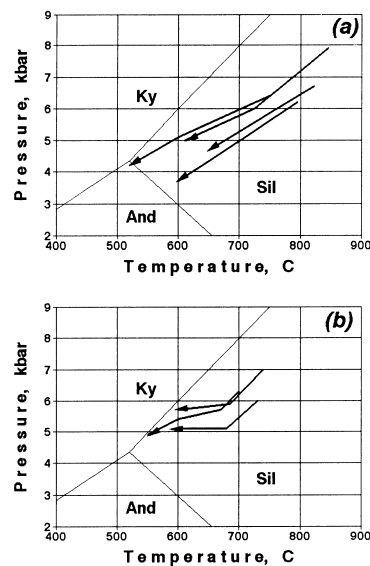


Fig. 1. Two types of  $P$ – $T$  paths for metapelites from the Limpopo complex calculated on the basis of thermobarometry (Perchuk et al., 1996): (a) decompression cooling, and (b) isobaric and near isobaric cooling.

differences in the geodynamic behavior of different crustal blocks of the Limpopo Belt during its emplacement in the crust. Certain crustal blocks were simply exhumed, allowing their adjustment to the normal thermal gradient of the crust during their emplacement (see  $P$ – $T$  paths in Fig. 1a). The exhumation of other blocks, however, was arrested at crustal levels of about 13–15 km, where they were rapidly cooled (see  $P$ – $T$  paths in Fig. 1b) because of the large temperature gradient between the hot granulites and the cooler underthrust greenstone wall rocks.

All these features provide a favorable background for a 2D numerical study of the formation and spatial distribution of rocks with different types of retrograde  $P$ – $T$  paths. This paper discusses 2D numerical modeling of  $P$ – $T$ -time paths for the exhumation of granulites located between two cratons.

## 2. Basic equations

The following differential equations were used for incompressible heat-conducting viscous flow in the gravitational field:

- Stockes equation of motion

$$\partial\sigma_{ij}/\partial x_j = \partial P/\partial x_i - \rho g_i, \quad (1)$$

where

$$\sigma_{ij} = \eta \varepsilon_{ij},$$

$$\varepsilon_{ij} = \partial v_i/\partial x_j + \partial v_j/\partial x_i,$$

- the continuity equation

$$\text{div}(\bar{v}) = 0; \quad (2)$$

- the heat conduction equation:

$$\partial T/\partial t - \Delta T \cdot k \cdot \rho^{-1} \cdot C_p^{-1} = \partial H/\partial t \cdot \rho^{-1} \cdot C_p^{-1} - \bar{v} \cdot \text{grad}(T), \quad (3)$$

where  $x$  is the coordinate, m;  $\bar{v}$  is velocity, m s<sup>-1</sup>;  $t$  is time, s;  $\sigma$  is viscous stress tensor, Pa;  $\varepsilon$  is strain rate tensor, s<sup>-1</sup>;  $P$  is pressure, Pa;  $T$  is temperature, K;  $\eta$  is viscosity, Pa s;  $\rho$  is density, kg m<sup>-3</sup>;  $g$  is acceleration within gravity field, m s<sup>-2</sup>;  $k$  is heat conductivity coefficient, W m<sup>-1</sup> K<sup>-1</sup>;  $C_p$  is isobaric heat capacity, J kg<sup>-1</sup> K<sup>-1</sup>;  $\partial H/\partial t$  is heat generation, W m<sup>-3</sup>; heat generation caused by viscous friction is equal to (Landau and Lifshitz, 1986)

$$\partial H_0/\partial t = 0.5\eta \varepsilon_{ij}^2 \quad (4)$$

where factor 0.5 corresponds to symmetry of tensor  $\varepsilon_{ij}$ ; for example, in case of pure 2D shear  $\partial H_0/\partial t = 0.5\eta(\varepsilon_{XY}^2 + \varepsilon_{YX}^2) = \eta \varepsilon_{XY}^2 = \eta \varepsilon_{YX}^2$ . Viscosity  $\eta$  is determined via a rheological equation. In the test of numerical solutions, the following two types of equations were used

$$\eta = \eta_0 \quad (5)$$

and

$$\eta = \eta_0 A / \left(1 + 0.5 \eta_0^2 \cdot A^2 \cdot \varepsilon_{ij}^2 \cdot \sigma_{cr}^{-2}\right)^B, \quad (6)$$

where

$$A = \exp[(\Delta E + P\Delta V)/RT],$$

$$B = (n - 1)/(2n),$$

$R = 8.313 \text{ J mol}^{-1}$ , gas constant;  $\eta_0$  is viscosity constant, Pa s;  $\Delta E$  is activation energy, J mol<sup>-1</sup>;  $\Delta V$  is activation volume, m<sup>3</sup> mol<sup>-1</sup>;  $n$  is power law constant;  $\sigma_{cr}$  is critical stress, Pa. Eq. (5) describes Newtonian flow whose viscosity does not depend on outer parameters. In contrast, Eq. (6) was empirically founded to describe the behaviour of viscous flow with  $P$ – $T$ -stress depending on rheology: if the stress tensor is essentially less than  $\sigma_{cr}$  the viscosity of the medium depends on  $P$  and  $T$  only; if the stress is much higher than the parameter  $\sigma_{cr}$ , we are dealing with  $n$ -power law rheology (Fig. 2). Such relationship corresponds to mantle material of  $\eta_0 = 1000 \text{ Pa s}$ ,  $\Delta E = 520,000 \text{ J/mol}$ ,  $\Delta V = 1.2 \cdot 10^{-5} \text{ m}^3/\text{mol}$ ,  $\sigma_{cr} = 3000 \text{ Pa}$ ,  $n = 3$ ; this material is characterized by diffusional creep at low ( $\ll 10,000 \text{ Pa}$ ) stress and by dislocational creep at high ( $\gg 100,000 \text{ Pa}$ ) stress (e.g. Turcotte and Shubert, 1982).

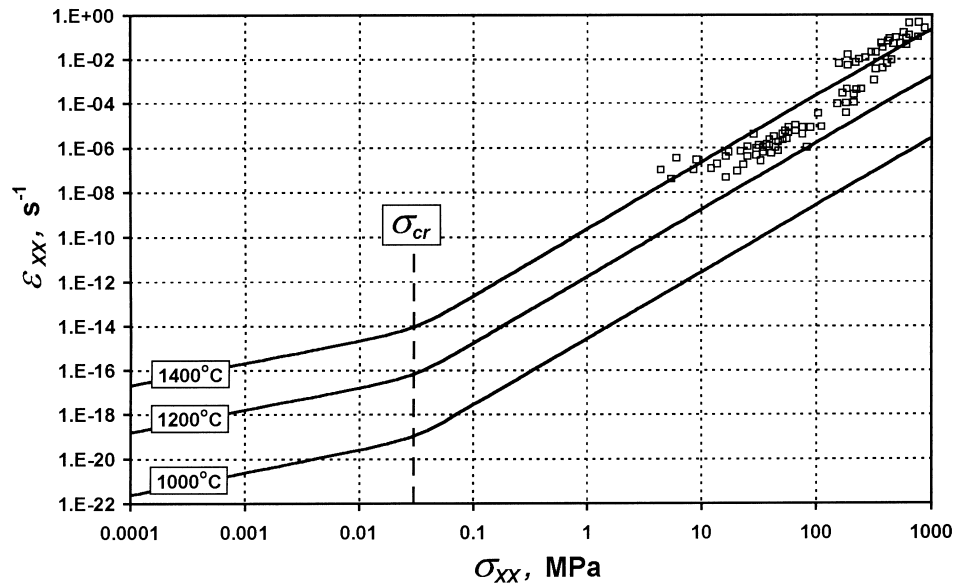


Fig. 2. The isotherms (solid lines) of stress dependence of the strain rate calculated with Eq. (6) with  $\eta_0 = 1000 \text{ Pa s}$ ,  $\Delta E = 500,000 \text{ J/mol}$ ,  $\Delta V = 0 \text{ m}^3/\text{mol}$ ,  $\sigma_{cr} = 30000 \text{ Pa}$ ,  $n = 3$ . The symbols show experimental data for olivine at  $T = 1400^\circ\text{C}$  (Ashby and Verall, 1977).

### 3. Methods of numerical modeling

The FDM on the regular rectangular non deforming (Eulerian) grid has been used to solve Eqs. (1)–(3). This method involves moving a field parameter (density, viscosity, etc.) with sharp discontinuities through a discrete mesh. The problem was solved by using a method of characteristics based on marker points. Weinberg and Schmelling (1992) developed an effective marker technique for multi-phase flow, where each phase has different rheological properties. Marker points, containing material property information are initially distributed on a regular rectangular (marker) grid with small ( $\leq \frac{1}{2}$  of marker grid distance) random displacement. The markers are moved through the mesh according to the velocity field.

Pressure values have been calculated for geometrical centers of cells, while temperatures and velocities were computed for nodes. The internal geometry of the grid is controlled by markers containing information on physical properties of the rocks. In the course of modeling we used the following five-step cyclic procedure:

1. Calculation of effective values of  $\eta$ ,  $\rho$ ,  $k$  and  $C_p$  for the nodes using the markers.
2. Calculation of pressure and velocity fields for a current moment  $t$  with relative accuracy better than  $10^{-4}$  by simultaneous iterative solution of Eqs. (1) and (2). The artificial compressibility was used for iterative pressure calculation

$$\Delta P = -a \operatorname{div}(v) \quad (7)$$

where  $\Delta P$  is an iteration correction for pressure, and  $a$  is an empirical coefficient (penalty method, Cuvelier et al., 1986).

3. Calculation of a value for time step,  $\Delta t$ , via given limits of change of  $v$ ,  $T$  and positions of markers within  $\Delta t$ ;
4. Determination of the temperature field for a new moment  $t + \Delta t$ , with relative accuracy better than  $10^{-6}$  by iterative solution of Eq. (3).
5. Determination of the positions of markers for a new moment  $t + \Delta t$ . The fourth order Runge–Kutta method was used for calculating the motion of markers using the velocity field.

### 4. Numerical modeling of $P$ – $T$ paths

We have developed a computer program to model a  $P$ – $T$  path for each given marker by using calculated temperature and pressure fields at each  $t = \text{const}$ . This allows the investigation of the shape of a path and the distribution of numerous  $P$ – $T$  paths in the modeled sequence. The comparison of such theoretically derived  $P$ – $T$  paths to those obtained from mineral geothermobarometry suggests an additional constrain for the control of geodynamic regimes of metamorphic and igneous complexes. In contrast to  $\rho$ ,  $k$  and  $C_p$  of the rocks, their effective viscosity vary significantly (within several orders) with  $P$ – $T$  parameters and depends on many other factors such as bulk stress, presence of water, presence of melt etc., which cannot always be estimated correctly. This limits the applicability of numerical modeling in terms of the

timing of different geodynamic processes. In many cases the problem can be tested by using independent geological, geochronological and petrological data.

The relative changes in the geometry of flow depends significantly on viscosity contrast values. Such values can be empirically found on the basis of comparison of the geometry of the model with the geological structure of modeled complexes (e.g. Weinberg and Shmelling, 1992). The evolution of the thermal field and the shape of modeled  $P$ – $T$  paths mainly depend on the relationship between convective and conductive heat flows. Taking into account relatively small (by comparison to  $\eta$ ) variations in  $\rho$ ,  $k$  and  $C_p$  of the rocks, these relationships are mainly defined by velocity fields and thus, by the absolute values of effective viscosities. These values can be empirically found by checking the consistency between the shapes of geothermobarometric and modeled  $P$ – $T$  paths. Preserving viscosity contrast and therefore a model geometry, we can vary absolute values of viscosities. This allows determining those values of effective viscosity which provide the best consistency between shapes of calculated and measured  $P$ – $T$  paths. Data on effective viscosities provide the correct timing of different stages of emplacement of a modeled magmatic or metamorphic complex. Thus, the accurate consistency of numerically modeled and empirically measured  $P$ – $T$  paths provides a way to calculate effective viscosities of the different crustal rocks in different geodynamic situations.

## 5. Test of numerical solutions

The accuracy of the numerical experiment has been tested by a comparison of numerical and analytical solutions for 2D flows. The major goal of the test was to check the applicability of the program for studies of the circulation of rocks within the Earth's crust and mantle. This requires an accurate solution of Eqs. (1)–(6) for multiphase fluid media with significant temperature gradients.

*The first series* of tests were done for the case of the Rayleigh–Taylor instabilities of a two-layer cross-section in the gravity field. Fig. 3a shows the initial geometry and boundary conditions for the modeled cross-section. We assumed that the initial sinusoidal disturbance of the boundary between layers is of a small amplitude ( $A$ ) and characteristic (Ramberg, 1981) wave length ( $\lambda$ ). This creates conditions to investigate the correct initial velocity of the diapir growth and the time dependence of its height.

Fig. 3b and c compare the numerical and analytical solutions. Fig. 3b demonstrates the numerical modeling of initial velocities for the growth of a diapir with the accuracy of  $\pm 5\%$ , which is almost dependant of the layer viscosity contrasts. This suggests correct numerical solutions of Eqs. (1) and (2). The results also suggest correct calculation of the effective values of  $\eta$  and  $\rho$  for the nodes using the markers in the case of sharp discontinuity. Fig. 3c shows similarities in numerical and analytical solutions for height of a diapir at the initial stage of its growth for a wide range of the viscosity contrasts ( $\eta_1/\eta_2 = 0.001 - 100$ ). This indicates a correct numerical procedure used for changing the geometry of a sequence (cross-section) and for time step estimation.

*The second series* of tests were conducted to check the numerical solution of the heat transfer Eq. (3). The calculations were done by using a model of the vertical flow of a heat-conductive medium of constant viscosity in a channel. Boundary conditions were taken as follows: given

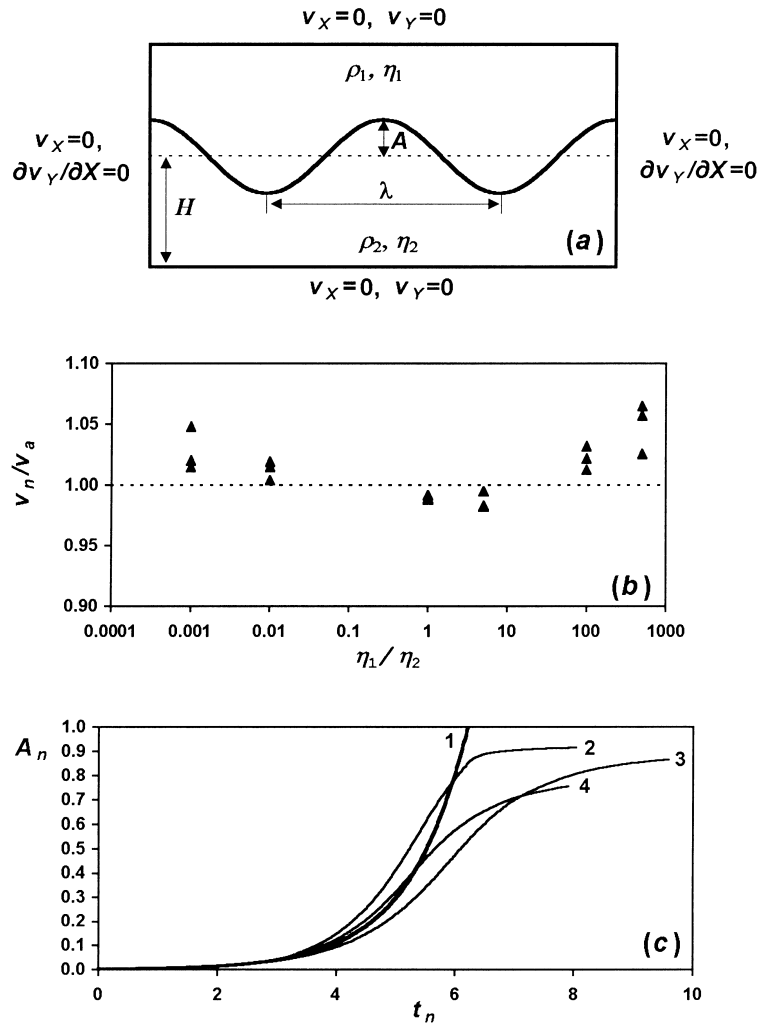


Fig. 3. The results of tests of numerical solutions for the case of the Rayleigh–Taylor instability of a two-layer cross-section in the gravity field. (a) initial geometry and boundary conditions for the modeled cross-section. (b) comparison of numerical ( $v_n$ ) and analytical ( $v_a$ ) solutions for initial velocities of growth of a diapir at the different values of  $\eta_1/\eta_2$  viscosity contrast. (c) dependency of non-dimensional height of a diapir ( $A_n = A/H$ ) from non-dimensional time [ $t_n = t \cdot K \cdot H \cdot g(\rho_1 - \rho_2)/(2\eta_2)$ , where  $K$  — factor of growth (Ramberg, 1981)]. Line 1: analytical solution. Lines 2–4: numerical solutions at the different values of viscosity contrast: 2 —  $\eta_1/\eta_2 = 10^{-3}$ , 3 —  $\eta_1/\eta_2 = 1$ , 4 —  $\eta_1/\eta_2 = 10^2$ .

vertical velocity ( $v_Y^0$ ) in the center of the channel entrance, non-slip conditions and  $T = T_0(Y) = \text{const}$  and  $\partial T/\partial Y = \partial T_0/\partial Y = \text{const}$  at the walls. The initial conditions were  $T = T_0(Y)$ ,  $\partial T/\partial X = 0$  and  $\partial T/\partial Y = \partial T_0/\partial Y$ . The horizontal steady-state profile for vertical velocities,  $v_Y(X)$ , is thus defined by the equation

$$v_Y(X) = -4v_Y^0/L^2(X^2 - LX), \quad (8)$$

where  $L$  is the width of the channel. The corresponding temperature distribution in the channel as a function of time is given by the following equation (Tikhonov and Samarsky, 1972)

$$T(X, Y, t) = T_0(Y) + \sum_{m=1}^{\infty} F_m E_{mt} \sin[\pi(2m - 1)X/L], \quad (9)$$

where

$$F_m = -8AL^2/[\pi(2m - 1)]^3,$$

$$E_{mt} = L^2/[\pi(2m - 1)]^2 \left\{ 1 - \exp\left(-[\pi(2m - 1)/L]^2 \kappa \cdot t\right) \right\} / \kappa, \quad \kappa = k/(\rho C p),$$

$$A = 4v_Y^0/L^2(\partial T_0/\partial Y),$$

where  $T(X, Y, t)$  is the temperature in the channel as a function of coordinates and time. Eq. (9) does not account for the heat production: for the first approximation, it is taken as negligible.

Diagrams in Fig. 4 show that the numerical and analytical solutions for both velocities and temperatures merge together, suggesting the correct procedure used for solutions of Eqs. (1)–(3).

A *third series* of tests were conducted to check the numerical solution of Eqs. (1) and (2) for flows with  $P$ – $T$ -stress dependent rheology under conditions of a significant temperature gradient. The computation was done for vertical flow of a viscous heat-conductive medium in a channel. Boundary conditions were taken as follows: given vertical velocity ( $v_Y^0$ ) in the center of the channel entrance, non-slip conditions and given temperatures  $T_l$  and  $T_r$  at the walls. The horizontal temperature distribution was defined according to the following equation (Fig. 5a)

$$\exp(-\Delta E/RT) = a + bX \quad (10)$$

where

$$a = \exp(-\Delta E/RT_l)$$

$$b = \exp(-\Delta E/RT_r) - a$$

where  $T_l$  and  $T_r$  are temperatures at the left and right walls of the channel. The condition  $\partial T/\partial Y = 0$  was defined for the vertical distribution of temperature. Eq. (6) describes viscosity for  $n = 3$ . Two principal cases with respect to Eq. (6) were investigated:

(i)  $\sigma_{cr} \gg \sigma_{XY}$ ; the following simplified *rheological equation* corresponds to this condition

$$\eta = \eta_0 \exp(\Delta E/RT) \quad (11)$$

while the analytical solution for the horizontal profile of  $v_Y$  within the channel was derived from Eqs. (1), (2), (10) and (11) as follows

$$v_Y(X) = (aC_1X^2/2 + aC_2X + bC_1X^3/3 + bC_2X^2/2)/\eta_0, \quad (12)$$

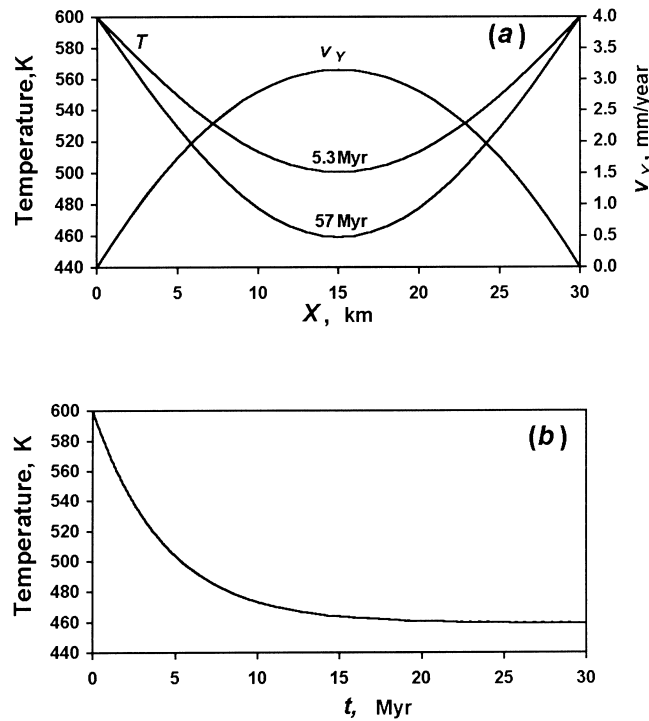


Fig. 4. The results of tests of numerical solutions for the case of vertical Newtonian (Eq. (5)) flow in the channel. The results of numerical (solid lines) and analytical (dashed lines) solutions merge together. Model parameters:  $k = 2$  W/m/K,  $\rho = 3000$  kg/m<sup>3</sup>,  $C_p = 1000$  J/kg/K,  $V_y^0 = 10^{-10}$  m/s,  $L = 30,000$  m,  $\partial T_0/\partial Y = 0.01$  K/m,  $T_0 = 600$  K. (a) horizontal temperature ( $T$ ) and vertical velocity ( $v_Y$ ) profiles. (b) time dependency of the temperature in the center of the channel.

(ii)  $\sigma_{cr} \ll \sigma_{XY}$  with the following simplified *rheological equation*

$$\eta = [\eta_0 \exp(\Delta E/RT) \cdot \sigma_{cr}^2 / (\partial v_Y / \partial X)^2]^{1/3} \quad (13)$$

while the analytical solution for horizontal profile of  $v_Y$  within the channel was derived from Eqs. (1), (2), (10) and (13) as follows

$$v_Y = (aC_1^3 X^4/4 + 3aC_1^2 C_2 X^3/3 + 3aC_1 C_2^2 X^2/2 + 3aC_2^3 X + bC_1^3 X^5/5 + bC_1^2 C_2 X^4/4 + 3bC_1 C_2^2 X^3/3 + bC_2^3 X^2/2) / (\eta_0 \sigma_{cr}^2), \quad (14)$$

where  $C_1$  and  $C_2$  are the coefficients, corresponding to the boundary conditions for  $v_Y$ .

Fig. 5b compares the numerical and analytical solutions for the horizontal distribution of velocities within the channel for the considered cases. It can be seen that the numerical and analytical solutions for velocities coincide well, suggesting that the correct procedure used for the numerical solutions of Eqs. (1) and (2).

Thus, the results of the tests show that the developed method can be applied for numerical

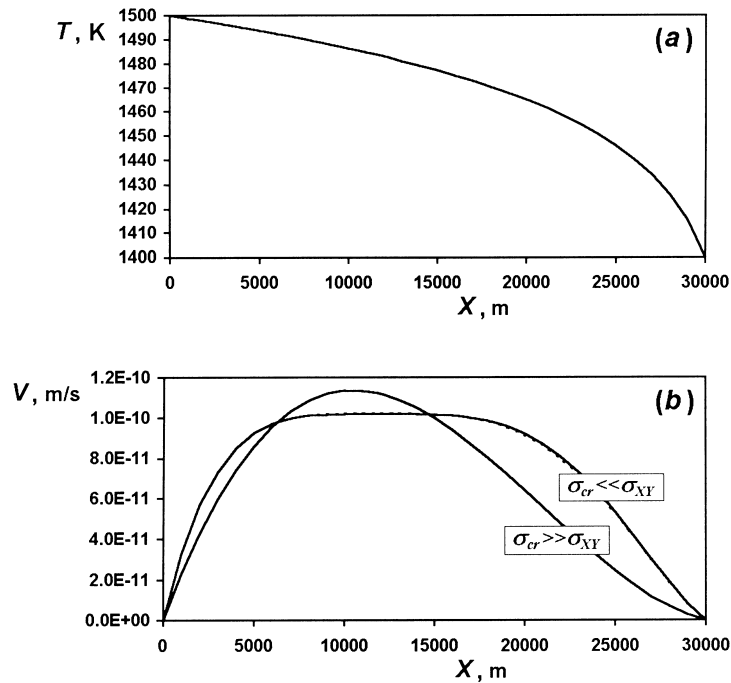


Fig. 5. The results of tests of numerical solutions for the case of vertical non-Newtonian (Eqs. (11) and (13)) flow in the channel with a horizontal temperature gradient given by Eq. (10). The results of numerical (solid lines) and analytical (dashed lines) solutions merge together. Model parameters:  $k = 2$  W/m/K,  $\rho = 3000$  kg/m<sup>3</sup>,  $C_p = 1000$  J/kg/K,  $v_y^0 = 10^{-10}$  m/s,  $L = 30,000$  m,  $T_i = 1500$  K,  $T_r = 1400$  K,  $\eta_0 = 1000$  Pa s,  $\Delta E = 520,000$  J/mol,  $\Delta v = 0$  m<sup>3</sup>/mol,  $n = 3$ . (a) horizontal temperature distribution calculated with Eq. (10). (b) velocity profiles ( $v = v_Y$ ) across the channel. Flow rheology is given by Eq. (11) ( $\sigma_{cr} \gg \sigma_{XY}$ ) and by Eq. (13) ( $\sigma_{cr} \ll \sigma_{XY}$ ).

modeling of the gravitational redistribution of material in the Earth's crust and mantle, including the simultaneous modeling of  $P$ – $T$  paths.

## 6. Model design and limitations

For the model design we used data (De Wit et al., 1992; De Wit and Ashwal, 1997) on the stratigraphy of the Kaapvaal craton in which the South Marginal Zone of the Limpopo granulite complex was emplaced. Fig. 6 shows a geometry of the 100 km wide and 30 km thick block of the initial cross-section used for modeling. The horizontal layering generally reflects the distribution of material within the craton with regard to compositions and densities. In spite of significant idealisation of the complex structure of the Kaapvaal craton (De Wit and Ashwal, 1997; De Beer and Stettler, 1992), the rock layering reflects both the small scale ( $\lambda = 2$ – $4$  km) and the large scale ( $\lambda = 10$ – $50$  km) gravitation instability of the cratonic successions, which provide development of polydiapirs (Weinberg and Shmelling, 1992). Sedimentary rocks of low density and viscosity compose the upper layers of the cross-section in Fig. 6. High density and viscosity mafic and ultramafic rocks of greenstone belts constitute 6–8 km thick

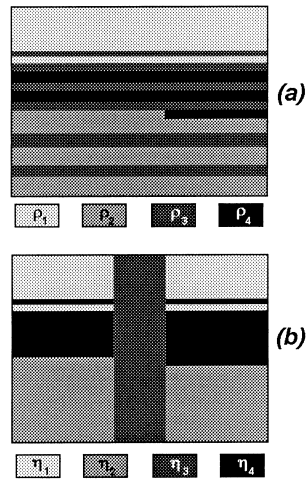


Fig. 6. Initial geometry of the modeled  $100 \times 30$  km cross-section. (a) distribution of densities: sediments (white),  $\rho_1 = 2700$  kg/m<sup>3</sup>; metapelites and gray gneisses (light gray),  $\rho_2 = 2800$  kg/m<sup>3</sup>; metabasites (dark gray),  $\rho_3 = 3000$  kg/m<sup>3</sup>; metakomatiites (black),  $\rho_4 = 3300$  kg/m<sup>3</sup>. (b) distribution of viscosities: sediments (white),  $\eta_1$ ; metapelites, gray gneisses and metabasites metamorphosed under conditions of granulite facies (light gray),  $\eta_2$ ; the rocks composing the 20 km wide shear zone (dark gray),  $\eta_3$ ; basalts and komatiites metamorphosed under conditions of green schist to amphibolite facies (black),  $\eta_4$ ;  $\eta_1/\eta_2/\eta_3/\eta_4 = 1/1/1/10^2$ .

rhythms representing the upper and partly middle portions of the succession. The gray gneiss unit at the lower portion of the succession in Fig. 6 is composed of rhythmic intercalation of tonalitic and basic material. The rocks of this unit are of intermediate density and low viscosity in comparison with the sediments and rocks of the greenstone belts. According to geophysical data, the Limpopo granulitic body in cross-section shows an asymmetrical shape (Roering et al., 1992; van Reenen and Smit, 1996). In order to reproduce this shape, for numerical modeling we used different numbers of ultramafic layers in the left and right portions of the cross-section. The initial weak zone at the contact of two cratons is given by a 20 km wide vertical zone of low viscosity of all rock types. The numerical modeling has been done for a Newtonian (Eq. (5)) fluid media with parameters and limitations as given in Table 1. Densities of the rocks were taken from Turcotte and Shubert (1982).

Table 1  
Parameters of numerical model (Fig. 8–Fig. 10)

Boundary conditions:	
Top	$T = 27^\circ\text{C}$ , $\partial v_X/\partial Y = 0$ , $v_Y = 0$
Bottom	$T = 927^\circ\text{C}$ (see $PT_{\max}$ in Fig. 1a), $v_X = 0$ , $v_Y = 0$
Walls	$\partial T/\partial X = 0$ , $v_X = 0$ , $v_Y = 0$
Initial conditions	$\partial T/\partial X = 0$ , $\partial T/\partial Y = \text{const} = 0.03$ K/m, $v_X = 0$ , $v_Y = 0$
Heat conductivity	$k = 4$ W/m/K
Isobaric heat capacity	$C_p = 1100$ J/kg/K

## 7. Results and discussion

Fig. 7 shows a scenario for gravitational redistribution of rocks in the Earth's crust. Both the presence of three major initial rhythms in the modeled stratigraphic succession and the difference in densities between layers of each rhythm provide acceleration of the process of gravitational redistribution (Perchuk et al., 1992). The interaction between rhythms and layers allows a rapid large-scale flow over the entire sequence. The development of the modeled cross-section clearly reflects thrusting of the relatively hot flattened granulitic diapir onto the relatively cold upper crustal cratonic rocks. According to the model of gravitational redistribution (Perchuk, 1989), the scenario of Fig. 7 may reflect evolution of many other Precambrian high grade terrains with greenstone rocks subducted under the granulites (e.g., Perchuk et al., 1989; Perchuk and Krotov, 1998).

Fig. 8 shows opposite directed movement of mafic and felsic material from different crustal levels: while granulites move up to the surface, cold metabasites and metakomatiites of the upper portion of the craton move down under hot granulites along the shear zone separating the two metamorphic terrains. The effect of shear heating calculated with Eq. (4) appeared to be insignificant and does not affect temperature distribution (Fig. 8). The formation of shear zones is associated with the development of a local convective cell that changes the movement

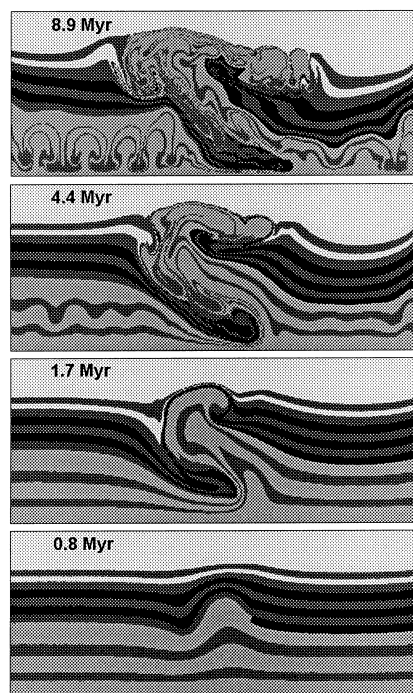


Fig. 7. Results of numerical modeling of the upward movement of a granulite diapir (gray body) generated under lower crustal conditions and the downward movement of an upper crustal greenstone sequence composed of metakomatiites (black), metabasalts (dark gray), and sediments (white). Initial model design and limitations correspond to Fig. 6 and Table 1.

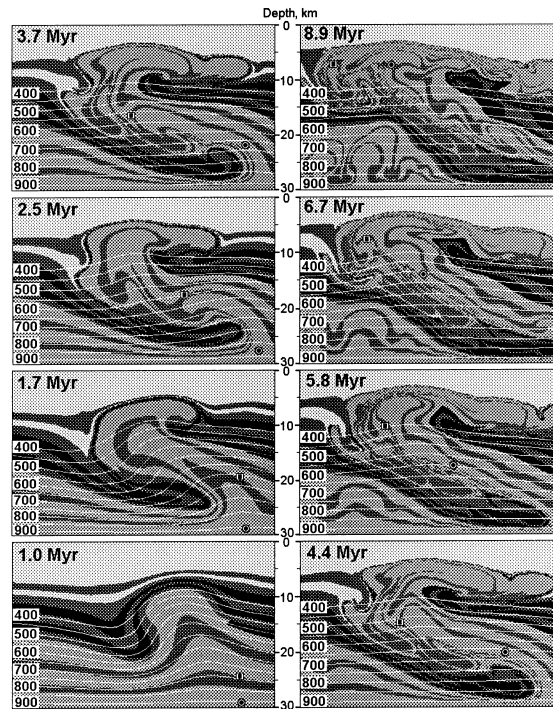


Fig. 8. Results of numerical modeling of movement of two granulitic fragments in a thermal and geometric field during the exhumation of the granulite diapir. Markers correspond to the fragments of decompression cooling (circle) and isobaric cooling (square)  $P$ – $T$  paths. Eight sketches  $40 \times 30$  km in size are taken from the  $100 \times 30$  km numerical model whose initial design and limitations correspond to Fig. 6 and Table 1. Isotherms are in  $^{\circ}\text{C}$ .

of some of the uprising granulite fragments: the square marker in Fig. 8 (1.7 and 2.5 Myr) moves from 700 to  $600^{\circ}\text{C}$  towards the downward moving cooler plate composed of greenstone material. This resulted in the near-isobaric portion of the  $P$ – $T$  path for the square marker (Fig. 9a). Another high-temperature deep-seated circle marker moves from isotherm  $900^{\circ}\text{C}$  directly (scenario in Fig. 8) to a sub-surface level along a common decompression-cooling  $P$ – $T$  path (Fig. 9a). At the final stage, both fragments appear at the same crustal level. Thus, difference in the initial position of a granulitic fragment of the primary succession (Fig. 8) results in different configurations of their  $P$ – $T$  paths (Fig. 9b and c), and in the rate of movement, decompression and cooling of these fragments within the uprising granulite diapir (Figs. 8 and 9b and c). The final position of fragments is consistent with their distribution within the Limpopo granulite complex: the fragment with isobaric cooling portions of its  $P$ – $T$  path is located close to the boundary of granulites with wall rocks, while the fragment with only decompression-cooling  $P$ – $T$  path is located in the core of the granulite body (Fig. 8, 8.9 Myr).

Figs. 10a and 11a illustrates the consistency of the modeled  $P$ – $T$  paths with those calculated on the basis of geothermobarometry (see Fig. 1) of the metapelites from the Limpopo granulite complex. This consistency is reached by adjustment of effective viscosities of the rocks. In other words, we used for geodynamic modeling effective viscosities that correspond to maximal consistency of the measured and the modeled  $P$ – $T$  paths (compare Figs. 10a–c and 11a–c). In

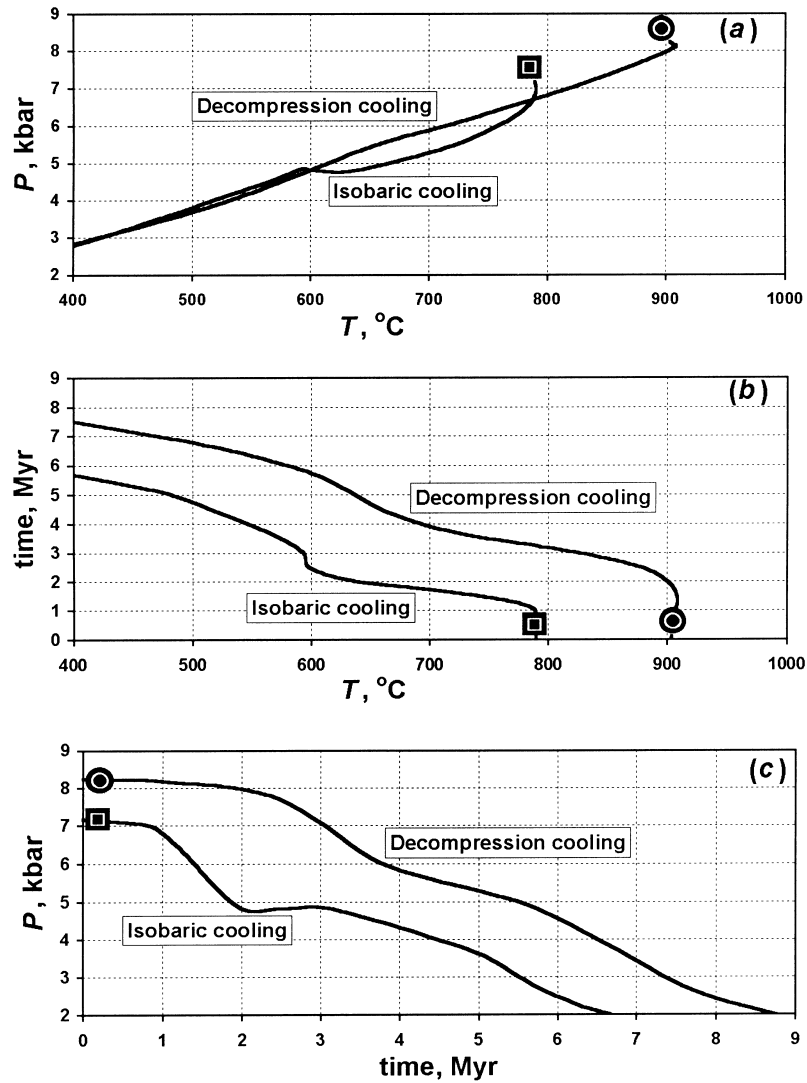


Fig. 9. The results of numerical modeling of  $P$ - $T$ -time paths for two granulitic fragments shown in Fig. 8. Diagrams (a), (b), and (c) respectively show  $T$ - $P$ , time- $T$ , and time- $P$  projections of the paths.

doing so, the following effective viscosities (Pa s) were obtained for the four rock types shown in Fig. 6b:  $\eta_1 = \eta_2 = \eta_3 = 10^{19}$ ,  $\eta_4 = 10^{21}$ . These values yield an average rate of exhumation of the granulites of the Limpopo belt as high as 2.5 mm/year. The calculated time of emplacement of the hot granulite body within the relatively cool Kaapvaal and Zimbabwe cratonic wall rocks is about 10 Myr.

The uncertainties of timing are defined by the  $k/(\rho \cdot C_p)$  ratio. This value depends on temperature, mineral compositions and texture of the rocks. The limits of variation of the ratio was calculated from data on  $k$  and  $\rho$  for the rocks under modeling (Turcotte and Shubert, 1982; Buntebarth, 1991) as well as data on  $C_p$  for minerals composing the rocks (Berman,

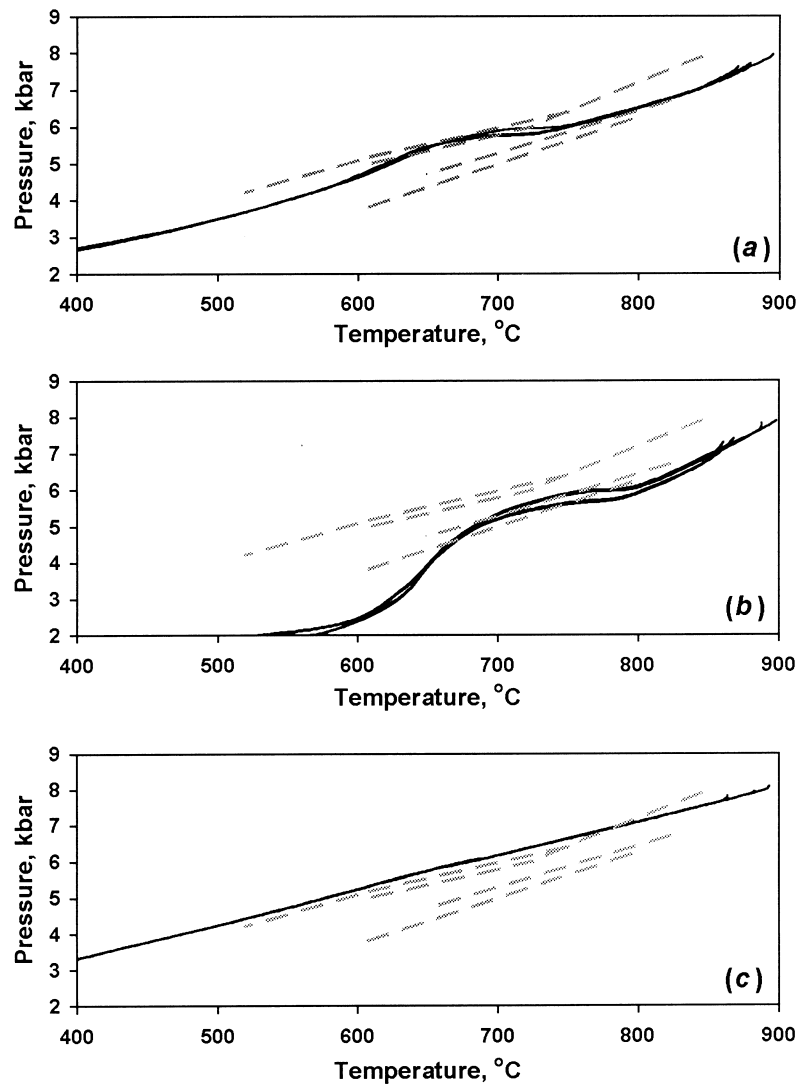


Fig. 10. The results of numerical modeling of decompression-cooling  $P$ – $T$  paths at different effective viscosities of the rocks. The results of modeling (solid lines) are plotted against the measured  $P$ – $T$  paths (dashed lines) of Limpopo granulites (see Fig. 1a). The geometry of the numerical model corresponds to that of Figs. 6 and 7. (a)  $\eta_1 = \eta_2 = \eta_3 = 10^{19}$ ,  $\eta_4 = 10^{21}$  Pa s. (b)  $\eta_1 = \eta_2 = \eta_3 = 10^{18}$ ,  $\eta_4 = 10^{20}$  Pa s. (c)  $\eta_1 = \eta_2 = \eta_3 = 10^{20}$ ,  $\eta_4 = 10^{22}$  Pa s.

1988). The ratio vary from 3 to 15  $\text{m}^2/\text{s}$  at  $T = 400$ – $900^\circ\text{C}$ . Therefore, absolute time estimations can vary within 1/2 order. Uncertainties of effective viscosities are defined by both the uncertainties of  $k/(\rho \cdot C_p)$  ratio and the uncertainties in initial distribution of densities (Fig. 6a). As a result, values of effective viscosity vary within one order.

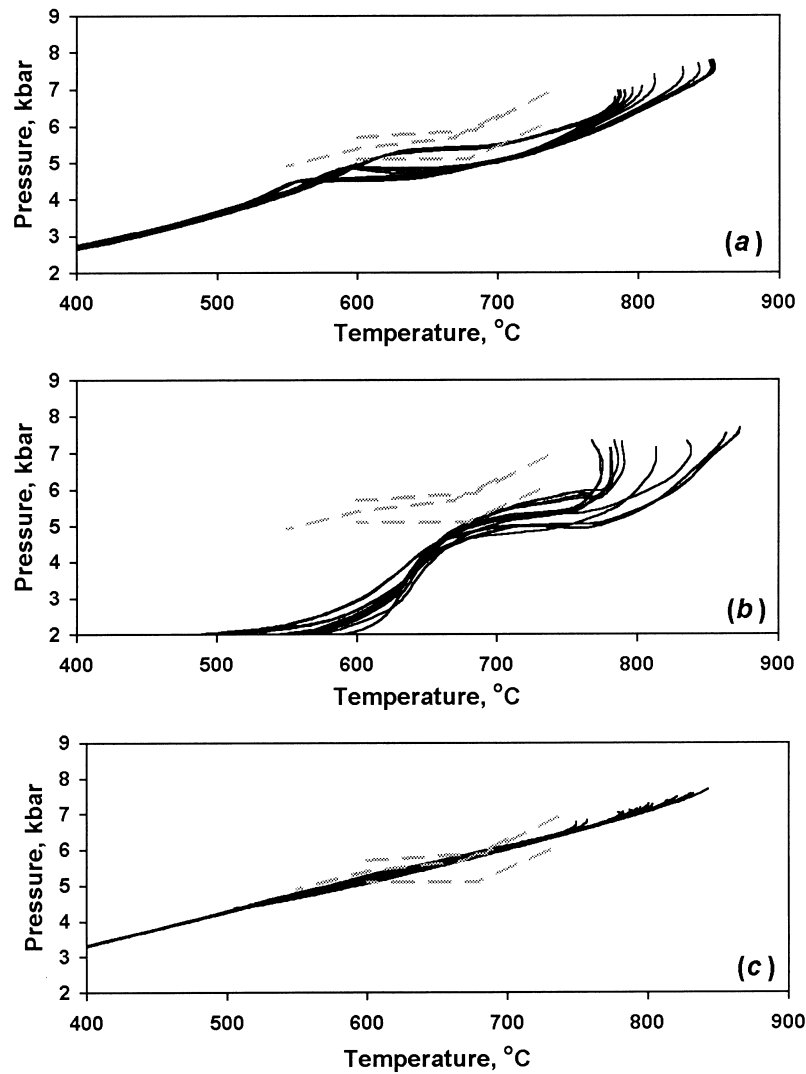


Fig. 11. The results of numerical modeling of near isobaric cooling  $P$ - $T$  paths at different effective viscosities of the rocks. The results of modeling (solid lines) are plotted against the measured  $P$ - $T$  paths (dashed lines) of Limpopo granulites (see Fig. 1b). The geometry of the numerical model corresponds to that of Figs. 6 and 7. (a)  $\eta_1 = \eta_2 = \eta_3 = 10^{19}$ ,  $\eta_4 = 10^{21}$  Pa s. (b)  $\eta_1 = \eta_2 = \eta_3 = 10^{18}$ ,  $\eta_4 = 10^{20}$  Pa s. (c)  $\eta_1 = \eta_2 = \eta_3 = 10^{20}$ ,  $\eta_4 = 10^{22}$  Pa s.

## 8. Conclusion

Two types of  $P$ - $T$ -paths, i.e., the one reflecting isobaric cooling and the other decompression cooling, observed in metapelites of Limpopo granulite complex (Fig. 1), were modeled by using 2D numerical experiments. The effective viscosities for uprising granulites and downward moving wall metabasites were estimated by checking the consistency between the shapes of measured and calculated paths. As a result, the effective viscosity of granulites was estimated

as high as  $10^{19}$  Pa s and about  $10^{21}$  Pa s for metabasites. The average rate of exhumation of granulites of the Limpopo complex was calculated to be about 2.5 mm/year.

Our 2D numerical experiments showed that the shape of a  $P$ – $T$  path for a given rock fragment is defined by its position in the initial pre-exhumation cross-section. The closer the fragment to the contact of the diapiric body, the higher its probability to be involved in the local circulation. Numerical modeling showed that the isobaric cooling  $P$ – $T$  path reflects interaction between the uprising hot granulite body on the one hand and the underthrust cool greenstone plate on the other. This interaction results in a local convective cell which causes sub-horizontal movement of granulitic material of the uprising diapir toward the cool plate. At a later stage, this material can join the principal flow of the uprising granulites recording a common decompression cooling  $P$ – $T$  path.

### Acknowledgements

This work was carried out as part of the RF-RSA scientific collaboration and through a RFBR support (grants # 99-05-65602 and # 96-15-98470 to LLP) and through the FRD and Gencor grants to DDVR. Authors are grateful to A.N. Polyakov (Montpellier University, France), G. Ranalli (Carleton University, Ottawa) and anonymous reviewer for comments and valuable suggestions.

### References

- Ashby, M.F., Verall, R.A., 1977. Micromechanisms of flow and fracture and their relevance to the rheology of the upper mantle. *Phil. Trans. R. Soc. Lond* 288 (A), 59–95.
- Berman, R.G., 1988. Internally-consistent thermodynamic data for minerals in the system  $\text{Na}_2\text{O}$ – $\text{K}_2\text{O}$ – $\text{CaO}$ – $\text{MgO}$ – $\text{FeO}$ – $\text{Fe}_2\text{O}_3$ – $\text{Al}_2\text{O}_3$ – $\text{SiO}_2$ – $\text{TiO}_2$ – $\text{H}_2\text{O}$ – $\text{CO}_2$ . *Journal of Petrology* 29 (2), 445–522.
- Buntebarth, G., 1991. Thermal model of cooling. In: Voll, G., Topel, J., Pattison, D.R.M., Seifert, F. (Eds.), *Equilibrium and Kinetics in Contact Metamorphism*. Springer–Verlag, Berlin, pp. 379–402.
- Cuvelier, C., Segal, A., Steenhoven, A.A., 1986. Finite element methods and Navier–Stokes equations. In: *Mathematics and its Applications*. D. Reidel, Dordrecht, Boston, Lancaster, Tokyo.
- De Beer, J.H., Stettler, E.H., 1992. The deep structure of the Limpopo belt from geophysical studies. *Precambrian Research* 55, 173–186.
- De Wit, M.J., Ashwal, L.D., 1997. *Greenstone Belts*. Clarendon Press, Oxford.
- De Wit, M.J., Roering, C., Hart, R.J., Armstrong, R.A., De Ronde, C.J., Green, R.W.E., Tredoux, M., Pederdy, E., Hart, R.A., 1992. Formation of an Archean continent. *Nature* 357, 553–562.
- England, P.C., Thompson, A.B., 1984. Pressure–temperature–time paths of regional metamorphism. Part I: Heat transfer during the evolution of regions of thickened continental crust. *Journal of Petrology* 25, 894–928.
- Harley, S.L., 1989. The origin of granulites: a metamorphic perspective. *Geological Magazine* 126, 215–231.
- Landau, L.D., Lifshitz, E.M., 1986. *Theoretical Physics; VI, Hydrodynamics*. Nauka, Moscow (in Russian).
- Perchuk, L.L., 1973. *Thermodynamic Regimes of Deep Seated Processes*. Nauka, Moscow (in Russian).
- Perchuk, L.L., 1977. Thermodynamic control of metamorphic processes. In: Saxena, S.K., Bhattacharji, S. (Eds.), *Energetics of Geological Processes*. Springer–Verlag, New York, pp. 285–352.
- Perchuk, L.L., 1989.  $P$ – $T$ -fluid regimes of metamorphism and related magmatism with specific reference to the Baikal Lake granulites. In: Daly, S., Yardley, D.W.D., Cliff, B. (Eds.), *Evolution of Metamorphic Belts*. Geological Society of London, London, pp. 275–291 Special Publication.

- Perchuk, L.L., Gerya, T.V., Nozhkin, A.D., 1989. Petrology and retrogression in granulites of the Kanskiy Formation, Yenisey Range, Eastern Siberia. *Journal of Metamorphic Geology* 7, 599–617.
- Perchuk, L.L., Gerya, T.V., van Reenen, D.D., Safonov, O.G., Smit, C.A., 1996. The Limpopo metamorphic complex, South Africa. Part II: Decompression and cooling regimes of granulites and adjacent rocks of the Kaapvaal craton. *Petrology* 4, 571–599.
- Perchuk, L.L., Krotov, A.V., 1998. Petrology of the mica schists of the Tanaelv belt in the southern tectonic framing of the Lapland granulite complex. *Petrology* 6 (2), 149–179.
- Perchuk, L.L., Podladchikov, Yu.Yu., Polaykov, A.N., 1992. *P–T* paths and geodynamic modelling some metamorphic processes. *Journal of Metamorphic Geology* 10, 311–319.
- Ramberg, H., 1981. Gravity, Deformation and the Earth's Crust. Academic Press, London, New York, Toronto, Sydney, San Francisco.
- Ranalli, G., 1995. Rheology of the Earth, 2nd ed. Chapman and Hall, London.
- Roering, C., van Reenen, D.D., De Wit, M.J., Smit, C.A., de Beer, J.H., van Schalkwyk, J.F., 1992. Structural geological and metamorphic significance of the Kaapvaal Craton–Limpopo Belt Contact. *Precambrian Research* 55, 69–80.
- Spear, F.S., 1993. Metamorphic Phase Equilibria and Pressure–Temperature–Time Paths. Min. Soc. America Publication, Washington, D.C.
- Tikhonov, A.N., Samarsky, A.A., 1972. Equations of Math Physics. Nauka, Moscow (in Russian).
- Thompson, A.B., England, P.C., 1984. Pressure–temperature–time paths of regional metamorphism. Part II: Their inference and interpretation using mineral assemblages in metamorphic rocks. *Journal of Petrology* 25, 929–955.
- Turcotte, D.L., Shubert, G., 1982. Geodynamics: Applications of Continuum Physics to Geological Problems. Wiley, New York.
- van Reenen, D.D., Roering C., Brandl G., Smit C.A., Barton, J.M., 1990. The granulite-facies rocks of the Limpopo Belt, South Africa. In: Vielzeuf, D., Vidal, Ph. (Eds.), *Granulites and Crustal Evolution*. NATO ASI Series (C): Mathematical and Physical Sciences 311, 257–289.
- van Reenen, D.D., Smit, C.A., 1996. The Limpopo metamorphic belt, South Africa. Part I: Geological setting and relationships of the granulite complex with the Kaapvaal and Zimbabwe cratons. *Petrology* 4, 562–570.
- Weinberg, R.B., Shmelling, H., 1992. Polydiapirs: multiwavelength gravity structures. *Journal of Structural Geology* 14, 425–436.